Redox Biology 83 (2025) 103641

Contents lists available at ScienceDirect

Redox Biology

journal homepage: www.elsevier.com/locate/redox

Cth/Mpst double ablation results in early onset fatty liver disease in lean mice

Antonia Katsouda [a,b,1], Maria Markou [a,c,1], Dimitrios Valakos [d], Ioannis Theodorou [a,c], Andreas Papapetropoulos [a,c,*]

[a] Clinical, Experimental Surgery and Translational Research Center, Biomedical Research Foundation of the Academy of Athens, Athens, Greece
[b] Division of Cardiovascular Medicine, Radcliffe Department of Medicine, University of Oxford, Oxford, United Kingdom
[c] Laboratory of Pharmacology, Faculty of Pharmacy, National and Kapodistrian University of Athens, Athens, Greece
[d] Center of Basic Research, Biomedical Research Foundation of the Academy of Athens, Athens, Greece

ARTICLE INFO

Keywords:
CTH
MPST
Sulfide
Steatosis
Fatty liver
MAFLD

ABSTRACT

Metabolic dysfunction-associated fatty liver disease (MAFLD), a condition that stems from hepatic lipid accumulation in the absence of liver damage and overt inflammation, has become the most common hepatic disorder worldwide. Hydrogen sulfide (H_2S), a gasotrasmitter, endogenously generated mainly by cystathionine-γ lyase (CTH), cystathionine-β synthase (CBS) and 3-mercaptopyruvate sulfurtransferase (MPST) enzymes, exhibits protective effect in steatosis. Herein, we have demonstrated that CTH and MPST play a central role in MAFLD pathogenesis. Young *Cth/Mpst* knockout (*Cth/Mpst*$^{-/-}$) mice, fed a normal diet, had increased liver mass caused by enhanced hepatic lipid accumulation. Decreased insulin and glucose sensitivity was observed in CTH/MPST-deficient mice. At the cellular level, CTH/MPST inhibition resulted in increased lipid deposition and glucose uptake in hepatocytes. Transcriptome analysis revealed significant upregulation of cholesterol biosynthesis and SREBP-related genes in the liver of *Cth/Mpst* $^{-/-}$ mice. Transcription factor enrichment analysis of differentially expressed genes between two genotypes, revealed a major impact of LXR, RXR and PPARA in the observed phenotype. Sulfide donor (SG1002) treatment attenuated the fatty liver disease of CTH/MPST-deficient mice. Our findings underline the importance of endogenously produced H_2S in the pathogenesis of MAFLD and introduce the *Cth/Mpst*$^{-/-}$ mouse as a new animal model of early onset hepatic steatosis.

1. Introduction

Metabolic-dysfunction associated fatty liver disease (MAFLD) is a leading cause of chronic liver disease globally. This condition covers a broad spectrum, from simple lipid accumulation in the liver (hepatic steatosis) to the more severe nonalcoholic steatohepatitis (NASH), which can further develop into liver fibrosis and cirrhosis [1]. The only FDA-approved treatment for noncirrhotic, non-alcoholic steatohepatitis with moderate to advanced fibrosis is the thyroid hormone receptor-β agonist resmetirom, that was approved in 2024 [2]. Fatty liver disease is also associated with an increased risk of developing type 2 diabetes mellitus and cardiovascular events [1]. The prevalence of MAFLD has been on the rise globally, with a recent meta-analysis indicating that 32 % of adults are affected by this condition [3]. This increase has paralleled the global surge in obesity and diabetes [4,5]. MAFLD is a complex condition shaped by a range of genetic and environmental influences, resulting in different manifestations of the disease and making drug development challenging [6]. The intricate nature of MAFLD requires intense research to understand disease-specific mechanisms and discover potential therapeutic targets.

Hydrogen sulfide (H_2S), an endogenously produced molecule with pleiotropic functions, has been suggested to exhibit protective effects in fatty liver disease [7,8]. Multiple sources contribute to H_2S levels in mammalian tissues, including both enzymatic and non-enzymatic processes [9]. The primary enzymes responsible for sulfide production in mammals include two key enzymes of the transsulfuration pathway, cystathionine-γ lyase (CTH) and cystathionine-β synthase (CBS), along with 3-mercaptopyruvate sulfurtransferase (MPST), an enzyme of the

* Corresponding author. Laboratory of Pharmacology, Department of Pharmacy, National and Kapodistrian University of Athens, Athens, University Campus Zografou, 15771, Greece.
E-mail address: apapapet@pharm.uoa.gr (A. Papapetropoulos).
[1] Equally contributing authors.

https://doi.org/10.1016/j.redox.2025.103641
Received 9 March 2025; Received in revised form 14 April 2025; Accepted 14 April 2025
Available online 15 April 2025
2213-2317/© 2025 Published by Elsevier B.V. This is an open access article under the CC BY-NC-ND license (http://creativecommons.org/licenses/by-nc-nd/4.0/).

minor cysteine degradation pathway [9–11]. CTH protein expression has been shown to be dramatically reduced in fatty liver of mice, as well as in liver biopsies from patients with nonalcoholic fatty liver disease [12]. *Cth* global or hepatocyte-specific deletion in mice leads to increased hepatic lipid deposition under high-fat diet (HFD) conditions [12,13]. Increased hepatic insulin resistance, and higher hepatic gluconeogenic ability were also reported in CTH-deficient mice with a steatosis phenotype [12]. HFD feeding or aging of *Mpst*$^{-/-}$ mice results in an exacerbated fatty liver phenotype [14]. Moreover, global deletion of *Mpst* results in reduced glucose/insulin sensitivity in obese mice [14] We have previously generated a mouse model of *Cth/Mpst* double knockout (*Cth/Mpst*$^{-/-}$) [15]. Herein, we sought to determine the impact of *Cth/Mpst* double ablation in mice on steatosis under baseline conditions.

2. Material and methods

2.1. Animal studies

C57Bl/6J mice were purchased from the Jackson Laboratory. *Cth/Mpst*$^{-/-}$ mice have been previously described [15]. All animals used for experimentation were bred/housed in individual ventilated cages, under specific pathogen-free, temperature controlled (22 °C) and 12h light/-dark cycle conditions in full compliance with the guidelines of the Federation of Laboratory Animal Science Association recommendations in the Laboratory Animal Unit of Biomedical Research Foundation of the Academy of Athens (BRFAA) and allowed free access to diets and water. All studies were performed on 8-12-week-old male mice, unless otherwise noted. The left lateral lobe was used to determine the weight of the liver. All experimental procedures reported here were approved by the veterinary authority of the Prefecture of Athens, in accordance with the National Registration (Presidential Decree 56/2013) in harmonization with the European Directive 63/2010.

2.2. HepG2 cell line culture

HepG2 cells (ATCC) were cultured in complete Dulbecco's Modified Eagle Medium (cDMEM): DMEM (41966-029, Gibco) supplemented with 10 % fetal bovine serum (FBS, 10270-106, Gibco), and 1 % penicillin/streptomycin (P/S, LM-A4118, Bio-Sera), and incubated at 37 °C, 5 % CO_2 and 21 % O_2.

2.3. Pharmacological approaches

To increase sulfide levels, SG1002 (Sulfagenix) was added in Chow Diet (CD, E157452-04, Ssniff) to achieve a dose of 80 mg/kg/day. Mice received the CD containing the sulfide donor for 4 weeks. Inhibition of CTH and MPST was achieved using PAG (P7888, Sigma-Aldrich) and IMST-3 (Molport) respectively. Hepatocytes were treated with 1 mM PAG in PBS (P04-36500; PAN-Biotech), and 50 μM IMST-3 dissolved in DMSO (A3672, PanReac AppliChem) for 48h. An equal amount of PBS/DMSO was added to the control group.

2.4. Knockdown approach

To silence the expression of *CTH* and *MPST* genes, an siRNA (s3712, s194616, Invitrogen) specific for each sequence was transfected in HepG2 cells using lipofectamine reagent (13778150, Invitrogen), according to the manufacture's protocol for 48h. The control group was transfected with a scramble siRNA (AM461, Invitrogen) under the same conditions.

2.5. Glucose, insulin, pyruvate tolerance tests

Glucose tolerance was determined by intraperitoneal (i.p.) administration of D-glucose (1 g/kg of body weight, G5767,Sigma-Aldrich) after fasting for 16h. Insulin tolerance was determined by i.p. injection of Humulin NPH (1U/kg, HI 0319, Lilly) after fasting for 4h. For pyruvate tolerance test, pyruvate was administrated (1.5 g/kg, i.p., P5280, Sigma-Aldrich) after fasting for 16h. Glucose levels were was measured before and 15, 30, 60, 90, and 120min after injection in blood drawn from a tail venesection using a handheld glucometer (Contour XT) and strips (Contour Next).

2.6. Alanine transaminase (ALT) serum levels

Blood was collected via cardiac puncture in mice. Samples were next centrifuged (3,500 rpm, 10min, 4 °C) and heparinized plasma was isolated. ALT levels were measured using a Beckman Coulter AU480 Clinical Chemistry Analyzer (OSR6107, Beckman Coulter).

2.7. H&E staining

Tissues were isolated and fixed in 4 % paraformaldehyde (P6148, Sigma-Aldrich) solution in PBS overnight, before paraffin embedding. Hematoxylin (95057-844, VWR) and eosin (95057-848, VWR) staining was performed following standard procedures. Images were obtained using a DM IRE2 microscope (Leica Biosystems).

2.8. Oil red O staining

Liver tissues were isolated, embedded in optimal cutting temperature compound (Tissue-Tek), and placed at −80 °C. Tissue cryosections were fixed in 10 % formalin solution (HT501128; Sigma-Aldrich) for 10min, and Oil Red O staining was performed using a 0.3 % Oil Red O (O0625; Sigma-Aldrich) in 60 % isopropanol solution (10 min), according to standard procedures. Cryosections were then stained with hematoxylin and imaged using a bright-field Leica DMLS2 microscope.

HepG2 cells were fixed in 10 % formalin solution (HT501128, Sigma-Aldrich) over night (O/N), rinsed with 60 % isopropanol, and staining was performed using a 0.3 % Oil Red O (O0625, Sigma-Aldrich) in 60 % isopropanol solution (15 min), according to standard procedures. Lipid accumulation levels were determined by Oil Red O absorption at 500 nm, after adipocyte destaining with 100 % isopropanol.

2.9. Glucose measurement

Glucose levels were determined in the cell cultures of HepG2 at the end of each experimental procedure, using 10 μl of medium and a handheld glucometer with strips.

2.10. Western blot analysis

Liver tissues were homogenized in lysis buffer containing: 150 mM NaCl (7760, Calbiochem), 1 % NP-40 (74385, Sigma-Aldrich), 0.5 % Na-deoxycholate (A1531,0025, AppliChem), 0.1 % SDS (A2572, PanReac AppliChem), 50 mM Tris-HCl, pH7.4 (T1503, Sigma-Aldrich), and 2mM EDTA (4005; Merck) supplemented with a cocktail of protease (PI, 5892970001, Roche) and phosphatase inhibitors (*Pho*I, 4906837001, Roche). Lysates were centrifuged and the protein concentration in the supernatants was quantified using the DC protein assay (BIO-RAD, 5000116). Samples were separated on 12 % SDS-PAGE and transferred to a nitrocellulose membrane (Macherey-Nagel; Düren, Germany). The membranes were blocked (5 % milk, PanReac AppliChem, A0830) and probed with the following antibodies: anti-GAPDH (10494-1-AP, Proteintech), anti-CBS (14787-1-AP, Proteintech), anti-CTH (12217-1-AP, Proteintech), anti-MPST (HPA001240, Atlas Antibodies), anti-ETHE1 (PA5-56040, Invitrogen), anti-TST (16311-1-AP, Proteintech), anti-SQRDL (17256-1-AP, Proteintech), anti-SREBP1 (sc-365514, Santa Cruz Biotechnology) and anti-SREBP2 (sc-13552, Santa Cruz Biotechnology). Immunoblots were next processed with anti-rabbit (AP132P, Merck) or anti-mouse (7076; Cell Signaling) secondary antibody and

visualized using the Western HRP substrate (Merck). Quantification of western blots was performed using ImageJ software (NIH Image, National Institutes of Health, United States).

2.11. Sulfide production measurements

Sulfide production capacity was measured in liver extracts by the lead acetate method as previously described [16,17]. In brief, 30 mg of pulverized tissue was homogenized in 1X passive lysis buffer (PLB, E1941, Promega) and centrifuged. The protein concentration was quantified in the supernatants using the DC protein assay (BIO-RAD, 5000116) followed by normalization via additional 1X PLB. Lead acetate assay was set up by initially preparing the reaction mixture, which consists of 10 mM L-cysteine (L-cys, 168149, Sigma-Aldrich), 10 mM L-homocysteine (L-hyc, 69453, Sigma-Aldrich) and 1 mM Pyridoxal 5′-phosphate (PLP, P9255, Sigma-Aldrich) in PBS. A total of 150 μL of this mixture was next placed into each well of a 96-well plate. 100 μg of protein sample or an equal volume of PBS was added to the respective wells. The plate was overlaid with lead acetate- (20 mM lead (II) acetate trihydrate; 467863, Sigma-Aldrich) embedded filter paper and incubated at 37 °C overnight. Sulfide production was calculated against a calibration curve of sodium sulfide (Na_2S, 1313-82-2, Sigma-Andrich, 0–100 μM). Quantification of the dark circles, due to the formation of lead sulfide on the filter paper, was performed using ImageJ densitometry analysis (NIH Image, National Institutes of Health, United States) via the IntDen function, after subtracting background levels obtained from reaction mixture-only wells with no protein sample added.

2.12. RNA isolation and gene expression analysis using qRT-PCR

Total Liver RNA was extracted from hepatocytes using TRIzol (15596026, Invitrogen) and treated with DNase I (AM2222, Invitrogen) according to the manufacturers' instructions. RNA (500 ng) was reverse transcribed with the PrimeScript RT Reagent Kit (RR037A, Takara). qRT-PCR was performed using KAPA SYBR Fast Master Mix (KK4618, Kapa Biosystems) in a CFX96 Touch Real-Time PCR Detection System (Bio-Rad). Gene expression levels were calculated according to $2^{-\Delta\Delta CT}$ method using *B-ACTIN* as internal control and ultimately normalized to the control group. Primer sequences are:

*B-ACTIN*_forward: 5′- ACA-GAG-CCT-CGC-CTT-TGC-C -3′
*B-ACTIN*_reverse: 5′- GAT-ATC-ATC-ATC-CAT-GGT-GAG-CTG-G -3′
*CTH*_forward: 5′- GCC-AGC-ACT-CGG-GTT-TTG-A -3′
CTH_reverse: 5′- ACC-TGT-TTG-TAC-AGT-ACT-TAG-CCC -3′
*MPST*_forward, 5′- CGC-CTT-CAT-CAA-GAC-CTA-CGA -3′
*MPST*_reverse: 5′- CCA-GGT-TCA-ATG-CCG-TCT-CG -3'.

2.13. RNA-seq and pathway enrichment analysis

Total liver RNA was extracted and treated with DNase as described above using TRIzol (15596026; Invitrogen) and treated with DNase I (AM2222; Invitrogen) according to the manufacturers' instructions. RNA-seq experiments were carried out in the Greek Genome Center (GGC) of the BRFAA. RNA-seq libraries were prepared with the NEBNext Ultra II Directional RNA Library Prep Kit for Illumina, with 1 μg of total RNA input. Library QC was performed with the Agilent bioanalyzer DNA1000 kit and quantitation with the qubit HS spectrophotometric method. Approximately, at least 20 million 101 bp Single-End reads were generated for each sample. Quality Control (QC) was performed on the FASTQ raw data file for each sample using the FASTQC software. FASTQ files were aligned to the *Mus musculus* mm10 genome using HISAT2. Counts were defined using the htseq-count command of HTSeq package v2.0.3 using "intersection non-empty" mode and the option "reverse" regarding the library strandness. The count files were used as input for DESeq2. Normalization was performed with the estimate size factor function followed by Differentially Expressed Genes (DEGs) analysis. As DEGs were classified those with a $\log_2$Fold-Change value less than −0.58 or greater than 0.58 and a p-adjusted of <0.05. Pathway and Gene Ontology analysis were performed using the EnrichR web tool and protein-protein interaction analysis was performed in StringDB (version 12.0)

2.14. Statistical analysis

Data are expressed as mean ± SEM. Student's unpaired two-tailed *t*-test was used for comparison between two groups, and one-way ANOVA was used to compare three or more groups followed by a post hoc test. All statistical calculations were made using Graphpad Prism statistical software. Sample sizes are reported in all figure captions. p-value was considered significant when it was less than 0.05.

3. Results

3.1. *Cth/Mpst*$^{-/-}$ mice exhibit a distinct hepatic steatosis phenotype

Mice lacking both *Cth* and *Mpst* were generated as previously described [15] and lack of CTH and MPST was confirmed in the liver of *Cth/Mpst*-deficient animals at the protein level (Fig. 1A). Lack of the two H_2S-producing enzymes doesn't lead to a compensatory increase in CBS protein levels (Fig. 1A). Similarly, no changes in the levels of the sulfide degrading enzymes ethylmalonic encephalopathy 1 protein (ETHE1), thiosulfate sulfurtransferase (TST) and sulfide quinone reductase (SQRDL) were evident in liver lysates of *Cth/Mpst*$^{-/-}$ mice (Fig. 1B). Reduced sulfide production in the liver of *Cth/Mpst*$^{-/-}$ mice was observed using the lead acetate method (Fig. 1C).

To explore the role *of Cth/Mpst* double ablation in fatty liver disease, WT and mutant male mice were allowed free access to normal chow diet, and livers were collected at 8 weeks of age. In male CTH/MPST-deficient mice, liver weight was increased and histological signs of steatosis were apparent (Fig. 1D and E). Mass measurements, H&E− and Oil Red O staining also revealed increased liver weight and greater tissue lipid content in young female *Cth/Mpst*$^{-/-}$ fed a CD (Fig. 1F and G). Taken together, our data provide evidence that genetic ablation of *Cth* and *Mpst* leads to an early steatosis phenotype.

3.2. CTH/MPST inhibition results in impaired glucose and insulin sensitivity

Despite the increased liver mass characteristic of double knockout mice, we observed no differences in their body weight at this young age compared to WT mice (Fig. 2A), proving that steatosis in *Cth/Mpst*$^{-/-}$ mice is not related to obesity. Glucose and insulin tolerance tests (GTT, ITT) in *Cth/Mpst*$^{-/-}$ mice indicated that *CTH/MPST* deficiency disrupted glucose homeostasis and lead to insulin resistance (Fig. 2B and C). In line with the increased hepatic fat accumulation, we observed enhanced gluconeogenesis in the double knockout mice after pyruvate administration (Fig. 2D).

At the cellular level, Oil Red O staining revealed greater lipid accumulation in the hepatocytes in the presence of the CTH and MPST inhibitors (Fig. 2E), confirming the results obtained from animal genetic model studies and suggesting that hepatocyte CTH/MPST are responsible for the observed *in vivo* phenotype. In addition, glucose levels were reduced in the supernatants of cells treated with PAG/IMST-3, indicating increased glucose uptake that could potentially increase lipogenesis (Fig. 2F). Similar results were observed by the simultaneous silencing of *CTH* and *MPST* in cultured hepatocytes (Fig. 2G); Oil Red O staining revealed that the knockdown of both enzymes increased the lipid content of HepG2 cells (Fig. 2H).

3.3. Cth/Mpst double ablation causes dysregulation of hepatic cholesterol homeostasis

We next sought to identify the mechanisms through which lack of

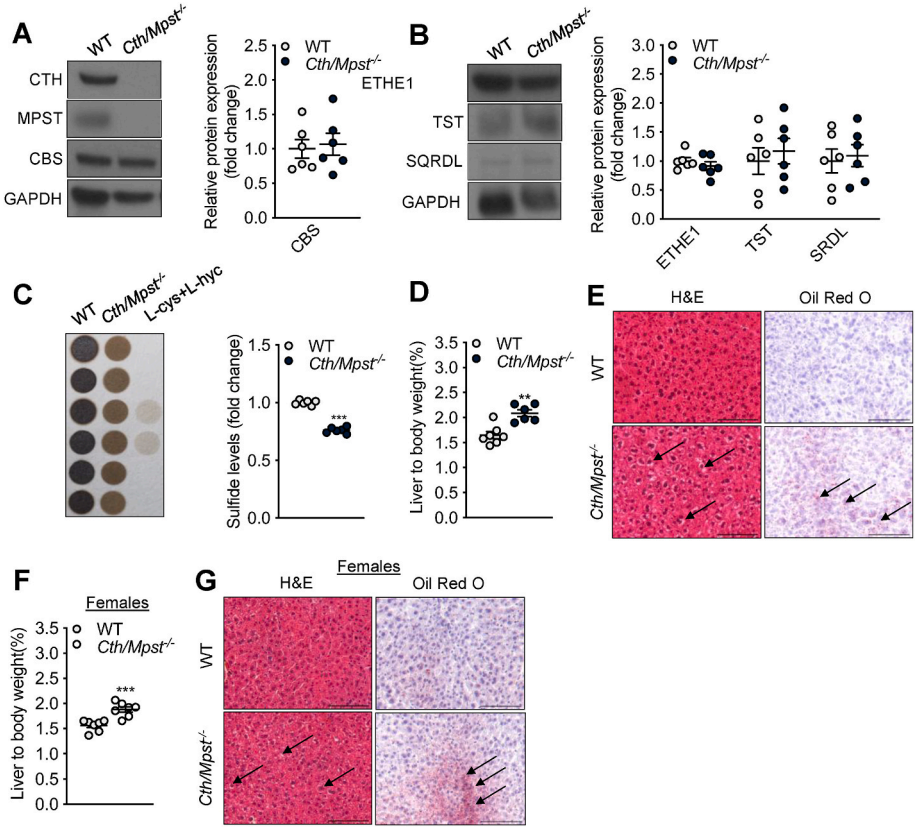

Fig. 1. *Cth/Mpst* double ablation leads to an early steatosis phenotype. Representative western blots and quantification of **(A)** CTH, MPST, CBS and **(B)** ETHE1, TST, SQRDL in liver of WT and *Cth/Mpst*$^{-/-}$ mice. **(C)** H_2S production capacity of liver extracts from WT or *Cth/Mpst*$^{-/-}$ mice in the presence of L-cysteine (L-cys) and L-homocysteine (L-hys). Data were obtained using the lead acetate method. Liver mass and representative photomicrographs from H&E– and Oil Red O- stained sections of the liver tissue of **(D, E)** male and **(F, G)** female WT and *Cth/Mpst*-deficient mice. Protein expression is presented as ratio over WT group (A, B). Sulfide levels are presented as ratio over WT group (C). Arrows indicate areas of increased lipid deposition. Data are presented as means ± SEM, $^{**}p \leq 0.01$, $^{***}p \leq 0.001$, N = 6–7 mice per group. Scale bar: 100 μm.

Cth/Mpst leads to fatty liver. To gain insight into the biological processes altered by *Cth/Mpst* deletion, RNA sequencing (RNA-seq) was performed using liver tissue from WT and *Cth/Mpst*$^{-/-}$ mice. Subsequent bioinformatic analysis revealed a plethora of differentially expressed genes (DEGs) between the two genotypes. The expression of 604 genes was significantly altered by *Cth/Mpst* deletion; 240 were upregulated and 264 were downregulated (Fig. 3 A). Gene Ontology (GO) analysis of the upregulated genes in *Cth/Mpst*$^{-/-}$ liver revealed sterol- and cholesterol-biosynthesis–related pathways among the most affected biological processes (Fig. 3B). Mevalonate kinase (*Mvk*), farnesyl diphosphate synthase (*Fdps*), ATP binding cassette subfamily A member 5 (*Abca5*), farnesyl-diphosphate farnesyltransferase 1 (*Fdft1*), 3-hydroxy-3-methyl-glutaryl-CoA synthase 1 (*Hmgcs1*), squalene epoxidase (*Sqle*) and glycerol-3-phosphate acyltransferase 1 (*Gpam*) were among the highest upregulated genes in mice lacking CTH/MPST (Fig. 3C). GO enrichment analysis of downregulated genes in *Cth/Mpst*$^{-/-}$ liver did not reveal significant alterations in biological processes (Fig. S1A, $-\log_{10}$(P-Adjusted)<1.3). Using the Reactome database, inhibition of CTH/MPST in the liver confirmed the upregulation of genes involved in cholesterol and lipid biosynthesis in double knockout mice and pointed towards the involvement of sterol regulatory-element binding proteins (SREBP; Fig. 3D). In line with this finding, we observed elevated protein levels of SREBP1 and SREBP2 proteins in the liver of *Cth/Mpst*$^{-/-}$ mice (Fig. 3E). SREBPs are known to directly activate the expression of more than 30 genes involved in the synthesis and uptake of cholesterol, fatty acids, triglycerides, and phospholipids [18]. In contrast, immune-related pathways were unaffected in hepatic tissue of deficient animals, since GO analysis did not reveal statistically significant terms ($-\log_{10}$(P-Adjusted<1.3) (Fig. S1B). This finding indicates that double KO mutant mice do not depict an acute or chronic inflammatory response in the liver.

To further investigate the molecular events connecting the lack of CTH/MPST with the massive transcriptome reprogramming observed in liver of *Cth/Mpst*$^{-/-}$ mice, transcription factor enrichment analysis of DEGs between two genotypes was performed. Based on publicly available data from the ChEA database regarding Chromatin Immunoprecipitation (ChIP) experiments in hepatic tissue, liver X receptors alpha (NR1H3, LXR), retinoid X receptors (RXR) and peroxisome proliferator activated receptor alpha (PPARA) play a pivotal role in transcriptome changes in fatty liver disease [19–24]. Analysis of our RNAseq data revealed that these transcription factors have a major impact gene expression in *Cth/Mpst*$^{-/-}$ mice on both up- and down-regulated genes (Fig. 3F, Fig. S1C). Expression levels of many LXR, RXR and PPARA target genes were altered in liver of *Cth/Mpst*$^{-/-}$ mice, further confirming the involvement of those transcription regulators in the observed phenotype (Fig. 3G). Protein-protein interaction network analysis predicts physical and indirect functional associations between LXR, RXR and PPARA (Fig. 3H)

3.4. Sulfide donor administration reverses the fatty liver phenotype of Cth/Mpst-deficient mice

CTH and MPST enzymes are significant sources of biologically active sulfide species. To assess whether the key role of CTH/MPST in the pathogenesis of fatty liver disease could be attributed to the altered generation of sulfide species, we next studied the consequences of

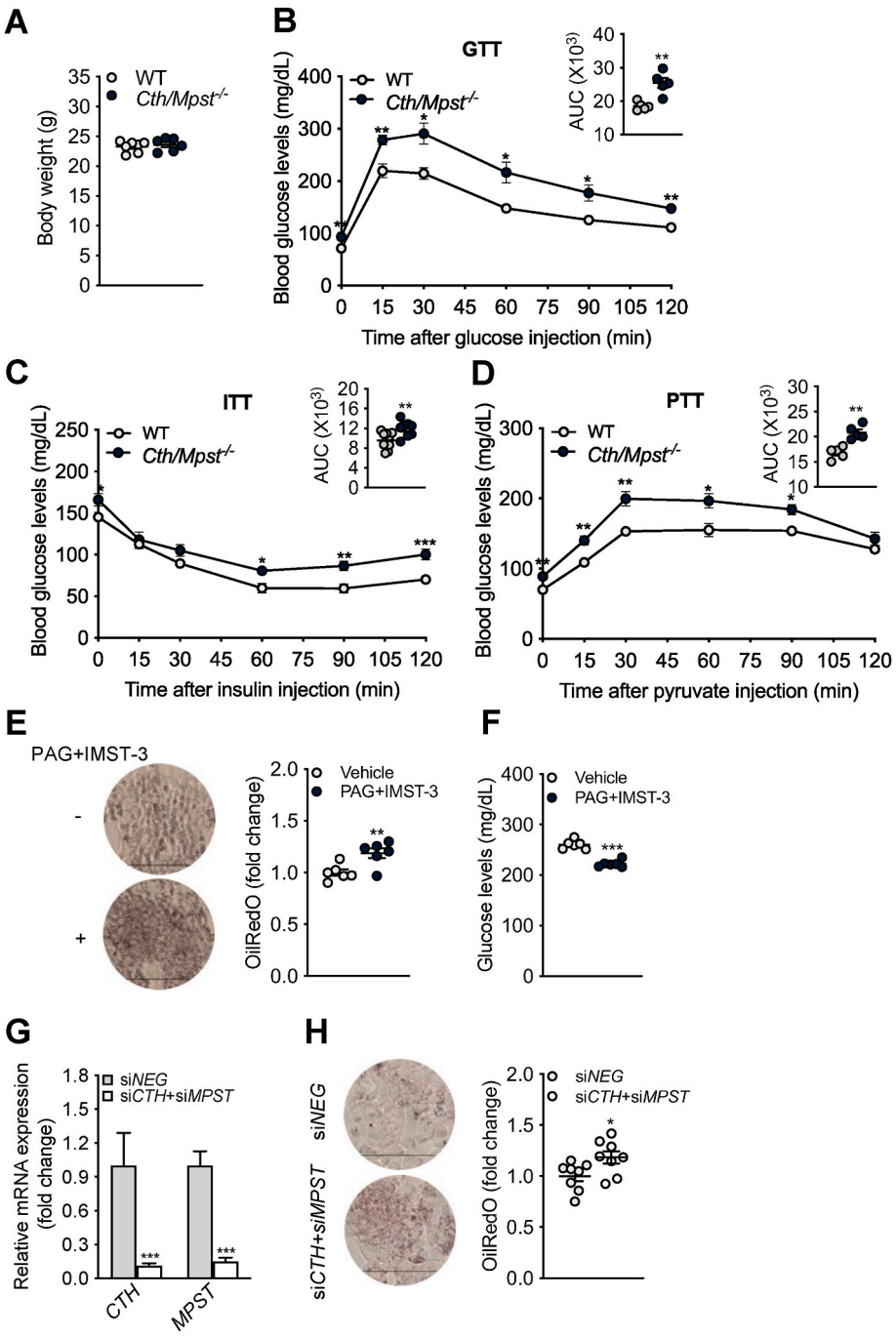

Fig. 2. ***Cth/Mpst*$^{-/-}$ mice are characterized by increased glucose, insulin and pyruvate tolerance.** **(A)** Body weight, **(B)** glucose (GTT), **(C)** insulin (ITT) and **(D)** pyruvate (PTT) tolerance tests in WT and *Cth/Mpst*$^{-/-}$ mice (AUC = area under the curve). **(E)** Photomicrographs and quantitation of lipid accumulation in hepatocytes in the presence or absence of a CTH inhibitor (PAG) and an MPST inhibitor (IMST-3). **(F)** Glucose levels in the supernatants of hepatocytes following the PAG and IMST-3 treatment. **(G)** *CTH* and *MPST* were knocked down in hepatocytes using silencing RNA for 48h. The reduction of enzyme expression after transfection was confirmed by real-time PCR. **(H)** Lipid accumulation was determined using Oil Red O in hepatocytes transfected with a control siRNA (si*NEG*) or a combination of siRNA targeting both the *CTH* and *MPST* genes. Optical density is presented as ratio over vehicle (E) or si*NEG* (H) group. mRNA levels are presented as ratio over si*NEG* group. (H) Data are presented as means ± SEM, $*p < 0.05$, $**p \leq 0.01$, $***p \leq 0.001$, (A) N = 6–7, (B, D) N = 5, (C) N = 8–10 mice per group, (E, F) N = 5–6, (G, H) N = 6–8 independent cell cultures. Scale bar: 200 μm (E) or (H) 150 μm.

treating the deficient mice with the sulfide donor SG1002. Double knockout mice were placed on chow diet (CD) containing the sulfide donor for 4 weeks. Administration of SG1002 reverses the increased liver mass of *Cth/Mpst*$^{-/-}$ mice (Fig. 4A). Reduced lipid accumulation in liver of animals given SG1002 was also evident by the results obtained from histological studies (Fig. 4B). Moreover, no differences in body weight of the animals receiving SG1002 was detected (Fig. 4C). The beneficial effect of SG1002 in fatty liver disease was further confirmed in *Cth/Mpst*$^{-/-}$ mice by ALT serum measurements; SG1002-treated *Cth/Mpst*$^{-/-}$ mice exhibit reduced levels of ALT (Fig. 4D).

4. Discussion

MAFLD, a common chronic liver disease characterized by lipid

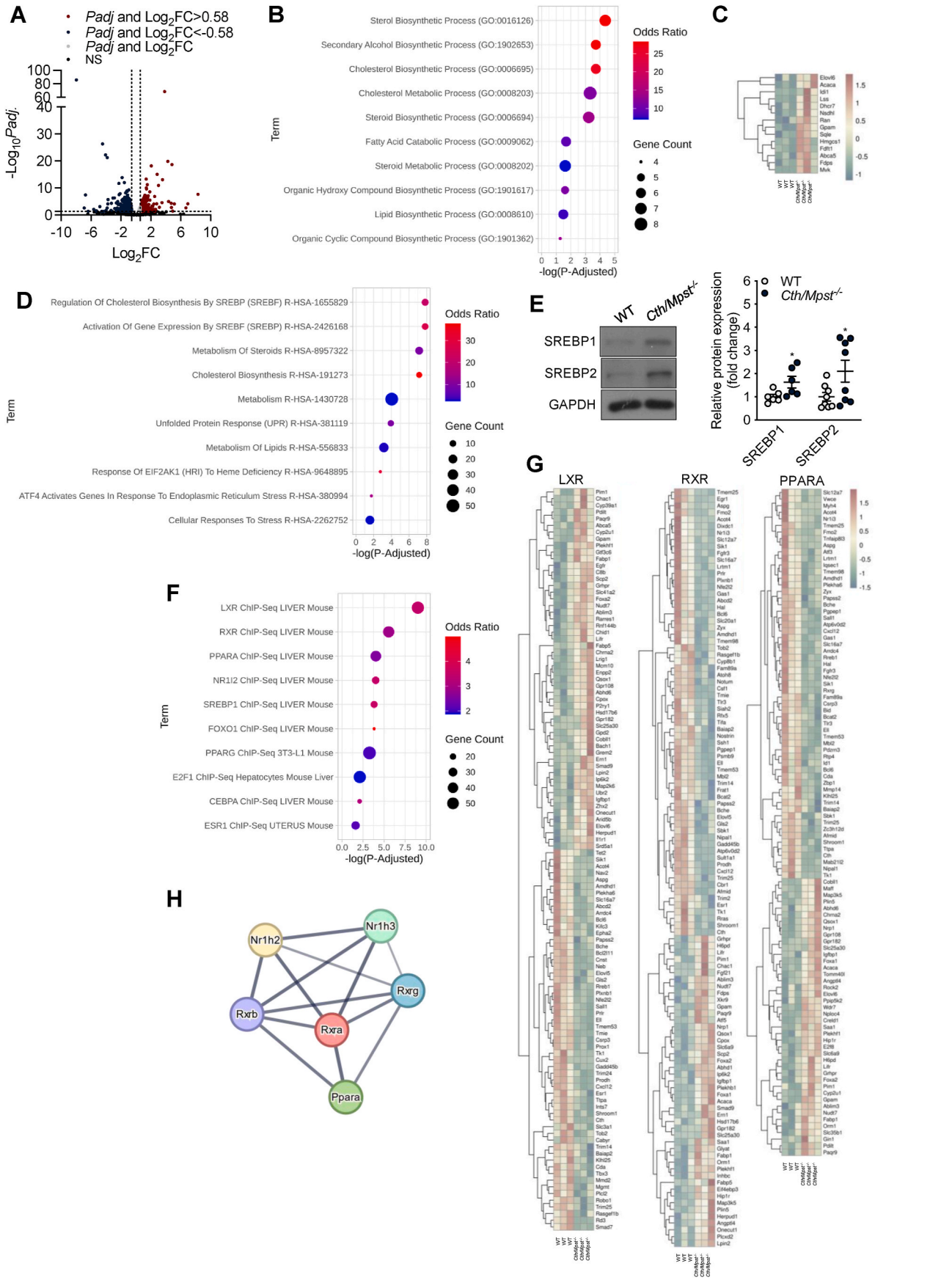

(caption on next page)

Fig. 3. Dysregulated cholesterol homeostasis in liver of *Cth/Mpst*$^{-/-}$ mice. **(A)** Volcano plot depicting the Differentially Expressed Genes (DEGs) in *Cth/Mpst*$^{-/-}$ as compared to wild-type mice. (Cut-offs for DEGs: $\log_2$FC>0.58, $\log_2$FC<-0.58, p-adjusted<0.05) and **(B)** Gene ontology (GO) enrichment analysis based on Biological Process of upregulated DEGs in liver of WT and mutant mice. **(C)** Heatmap depicting expression levels (z score) of the genes related to cholesterol biosynthesis pathway. **(D)** GO enrichment analysis based on the Reactome database of the upregulated DEGs in liver of *Cth/Mpst*$^{-/-}$ mice. **(E)** Representative western blots and quantitation of SREBP1 and SREBP2 proteins in the liver of WT and *Cth/Mpst*-double ablated mice. **(F)** Enrichment analysis regarding Transcription Factor Targets for upregulated genes performed using ChEA database from Enrichr webtool. **(G)** Heatmap illustrating changes in gene expression levels (z-score) of LXR-,RXR and PPARA-target genes in liver of WT vs. *Cth/Mpst*$^{-/-}$. **(H)** Protein-protein interaction network of enriched TFs in liver of *Cth/Mpst*-deficient mice. Data were obtained from RNA-seq (A-D, F, G). Protein expression is presented as ratio over WT group (E). (A-D, F, G) Data are presented as means ± SEM (E), *$p \leq 0.05$, (A-D, F, G) N = 3, (E) N = 6–8 mice per group.

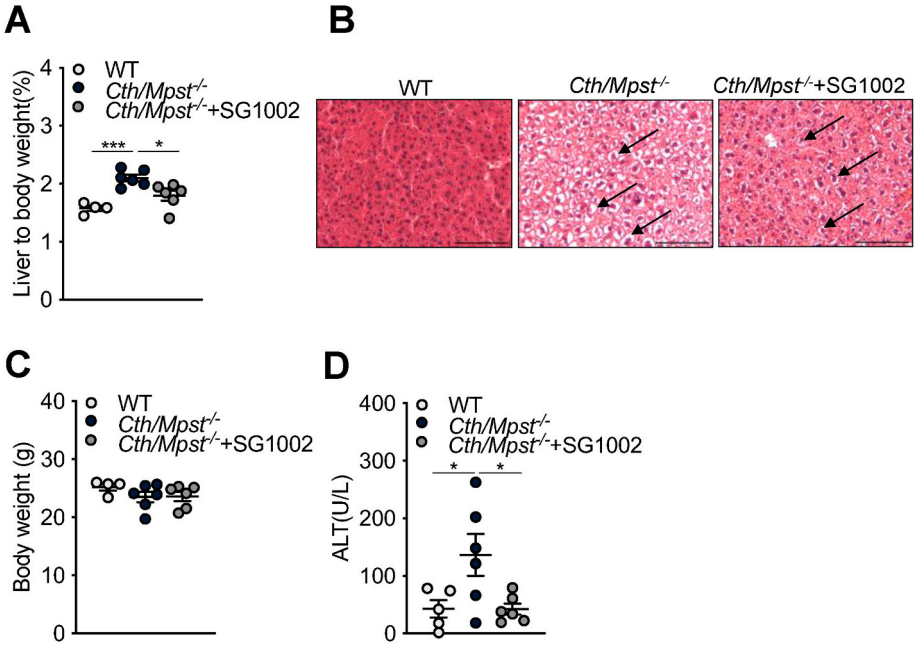

Fig. 4. Therapeutic administration of a sulfide donor reduces *Cth/Mpst*-deficient-induced steatosis. *Cth/Mpst*$^{-/-}$ mice were fed a drug-free chow diet (CD) or a CD containing the sulfide donor SG1002 for 4 weeks. Based on daily chow consumption, mice received 80 mg/kg SG1002. **(A)** Liver mass, **(B)** representative photomicrographs of liver sections stained with H&E, **(C)** body weight and **(D)** ALT serum levels in CD mice with or without SG1002 treatment. Data are presented as means ± SEM, *$p < 0.05$, ***$p \leq 0.001$, N = 4–6 mice per group. Scale bar: 100 μm.

accumulation in hepatocytes, contributes to the development of cirrhosis, hepatocellular carcinoma, and type 2 diabetes [25]. Previous work from our group has shown that MPST ablation results in enhanced fatty liver in mice placed on high-fat diet [14]. A similar phenotype has been observed in CTH-deficient mice [12,13]. We, thus, set out to investigate whether double ablation of CTH/MPST could lead to steatosis, serving as a novel genetic model of MAFLD.

Young *Cth/Mpst*$^{-/-}$ mice, fed a normal diet, exhibit hepatic lipid deposition, elevated liver mass, increased insulin resistance and reduced glucose tolerance. It should be noted that deletion of *Cth* or *Mpst* individually does not result in increased liver weight and steatosis in young mice fed a normal diet [13,26,27]. Although the regulatory role of endogenously produced H_2S in steatosis has been investigated, published studies are limited to diet-induced models of MAFLD. The present study extends the knowledge on the effect of H_2S also on the pathogenesis of steatosis in lean mice. It should be noted that elevated glucose levels were detected in *Cth/Mpst*$^{-/-}$ mice after pyruvate administration. Increased gluconeogenesis has previously been reported in HFD-fed *Cth* knockout mice [27].

RNA-seq analysis revealed that liver steatosis in *Cth/Mpst*$^{-/-}$ mice was accompanied by upregulation in cholesterol biosynthesis-related pathways mice. In line with this observation, we found increased liver protein levels of SREBP1 and SREBP2 in the liver of *Cth/Mpst*$^{-/-}$ mice. SREBP1 preferentially increases the expression of enzymes in the fatty acid biosynthetic pathway, while SREBP2 drives cholesterologenesis [28–30]. SREBP2–responsive genes include HMG-CoA synthase, HMG-CoA reductase, farnesyl diphosphate synthase, and squalene synthase, while SREBP1 increases the transcription of ATP-citrate lyase, acetyl-CoA carboxylase, fatty acid synthase, a rate-limiting enzyme of the fatty acid elongase complex, stearoyl-CoA desaturase, and glycerol-3-phosphate acyltransferase, which initiates triglyceride and phospholipid biosynthesis [18]. Transcripts for most of these enzymes were found to be increased in *Cth/Mpst*$^{-/-}$ mice. It should be noted that dysregulated cholesterol metabolism has been associated with the severity of fatty liver disease [31]. In addition, a plethora of LXR-, RXR- and PPARA-target genes were also among the DEGs in hepatic tissue of WT vs. *Cth/Mpst*$^{-/-}$ mice, indicating their involvement in the hepatic transcriptome changes. Interestingly, LXR is known to upregulate SREBP1 expression [32]. Our data are in line with previous observations indicating the regulatory role of LXR, RXR and PPARA in cholesterol homeostasis and hepatic lipid accumulation [19–24]. Among the DEGs, we observed 32 genes (14 that are upregulated and 18 that are downregulated) that are shared targets for LXR, RXR and PPARA; NRF2 (Nfe2l2), which is protective against liver steatosis, is found among the downregulated genes [33].

Preclinical murine models of MAFLD include both diet-induced and genetically modified models, while chemical-induced models are mainly used to study later stages of the disease including the transition from non-alcoholic steatohepatitis (NASH) to cirrhosis [34,35]. Diet-induced models, such as high-fat, high-cholesterol or high-fructose diets, closely mimic the nutritional causes of MAFLD in humans and are useful for studying the role of the metabolic syndrome in disease progression.

However, the development of the disease requires a relatively long period of time; mice fed a high fat diet (45 % energy from fat) develop fatty liver after 12 weeks. In addition, experimental animals show heterogeneity in phenotypic characteristics [36]. Regarding the genetically modified models, the most prevalent models of steatosis are those that affect leptin signaling. *Db/db* (homozygous for the autosomal recessive diabetic gene (*db*), encoding a point mutation that leads to a lack of the long isoform of the leptin receptor), and *ob/ob* (autosomal recessive mutation in the leptin gene that encodes a truncated and non-functional leptin) mice exhibit obesity, insulin resistance, and significant hepatic steatosis. They are commonly used to study the metabolic aspects of MAFLD, however, since they show significant weight gain from the first 3 weeks of life, their use is limited to studies of steatosis in the context of obesity [37]. Transgenic mice that overexpress human patatin-like phospholipase domain-containing 3 (PNPLA3), 148 M variant (*PNPLA3*^{I148M}) and Gankyrin (Gank)-deficient mice have also been reported as murine models of MAFLD, however exposure to special diets is required to induce hepatic lipid accumulation [38,39]. In our study, we introduce a novel model of MAFLD that develops pronounced hepatic steatosis along with impaired glucose tolerance and insulin resistance. The *Cth/Mpst*$^{-/-}$ mouse outperforms other MAFLD models in developing fatty liver at a young age without exposure to a special diet. Another advantage of the *Cth/Mpst*-deficient mouse model is that it mimics human lean-MAFLD. As with any animal model, the present model has limitations as it fails to fully replicate the complexity of human MAFLD, which involves a multifactorial interaction of genetics, diet, lifestyle, and environmental factors. More detailed experiments aimed at studying the molecular mechanism triggering steatosis in *Cth/Mpst*$^{-/-}$ mice, along with experiments investigating aspects of mitochondrial biology and bioenergetic measurements could offer additional insights regarding the mechanisms involved in the observed phenotype.

5. Conclusion

We conclude that CTH/MPST/H_2S are involved in the pathogenesis of MAFLD and that double deficient mice can be used in drug target identification and preclinical screening of drug candidates for MAFLD.

CRediT authorship contribution statement

Antonia Katsouda: Writing – review & editing, Writing – original draft, Visualization, Validation, Methodology, Investigation, Formal analysis, Data curation, Conceptualization. **Maria Markou:** Writing – review & editing, Validation, Methodology, Investigation. **Dimitrios Valakos:** Writing – review & editing, Visualization, Validation, Investigation, Formal analysis, Data curation. **Ioannis Theodorou:** Writing – review & editing, Visualization, Methodology, Formal analysis, Data curation. **Andreas Papapetropoulos:** Writing – review & editing, Writing – original draft, Validation, Supervision, Resources, Project administration, Investigation, Funding acquisition, Data curation, Conceptualization.

Declaration of Competing interest

The authors declare that the research was conducted in the absence of any commercial or financial relationships that could be construed as a potential conflict of interest.

Acknowledgements

The authors would like to thank the Director (Dr. Kostomitsopoulos) and the personnel of the BRFAA animal facility for their professionalism and their valuable help in breeding and maintaining the animal lines used in the study and Dr. Vassilis Aidinis for the ALT measurements. The research project was implemented in the framework of H.F.R.I Call "Basic research Financing (Horizontal support of all Sciences)" under the National Recovery and Resilience Plan "Greece 2.0" funded by the European Union –NextGenerationEU (H.F.R.I. Project Number:15768).

Appendix A. Supplementary data

Supplementary data to this article can be found online at https://doi.org/10.1016/j.redox.2025.103641.

Data availability

Data will be made available on request.

References

[1] N. Chalasani, Z. Younossi, J.E. Lavine, M. Charlton, K. Cusi, M. Rinella, S. A. Harrison, E.M. Brunt, A.J. Sanyal, The diagnosis and management of nonalcoholic fatty liver disease: practice guidance from the American association for the study of liver, Diseases 67 (2018) 328–357, https://doi.org/10.1002/hep.29367/suppinfo.

[2] S. Topouzis, A. Papapetropoulos, S.P.H. Alexander, M. Cortese-Krott, D.A. Kendall, K. Martemyanov, C. Mauro, N. Nagercoil, R.A. Panettieri, H.H. Patel, R. Schulz, B. Stefanska, G.J. Stephens, M.M. Teixeira, N. Vergnolle, X. Wang, P. Ferdinandy, Novel drugs approved by the EMA, the FDA and the MHRA in 2024: a year in review, Br. J. Pharmacol. 182 (2025) 1416–1445, https://doi.org/10.1111/bph.17458.

[3] K. Riazi, H. Azhari, J.H. Charette, F.E. Underwood, J.A. King, E.E. Afshar, M. G. Swain, S.E. Congly, G.G. Kaplan, A.A. Shaheen, The prevalence and incidence of NAFLD worldwide: a systematic review and meta-analysis, Lancet Gastroenterol Hepatol 7 (2022) 851–861, https://doi.org/10.1016/S2468-1253(22)00165-0.

[4] A. Afshin, M.H. Forouzanfar, M. Reitsma, P. Sur, K. Estep, A. Lee, L. Marczak, A.H. Mokdad, M. Moradi-Lakeh, Health Effects of Overweight and Obesity in 195 Countries over 25 Years. GBD 2015 Obesity Collaborators, N. Engl. J. Med. 377 (n. d.) 13–27. https://doi.org/10.1056/NEJMoa1614362.

[5] N. Stefan, K. Cusi, A global view of the interplay between non-alcoholic fatty liver disease and diabetes, Lancet Diabetes Endocrinol. 10 (2022) 284–296, https://doi.org/10.1016/S2213-8587(22)00003-1.

[6] S.L. Friedman, B.A. Neuschwander-Tetri, M. Rinella, A.J. Sanyal, Mechanisms of NAFLD development and therapeutic strategies, Nat. Med. 24 (2018) 908–922, https://doi.org/10.1038/s41591-018-0104-9.

[7] L. Sun, S. Zhang, C. Yu, Z. Pan, Y. Liu, J. Zhao, X. Wang, F. Yun, H. Zhao, S. Yan, Y. Yuan, D. Wang, X. Ding, G. Liu, W. Li, X. Zhao, Z. Liu, Y. Li, Hydrogen sulfide reduces serum triglyceride by activating liver autophagy via the AMPK-mTOR pathway Hydrogen sulfide reduces serum triglyceride by activating liver autophagy via the AMPK-mTOR pathway, Am. J. Physiol. Endocrinol. Metab. 309 (2015) E925–E935, https://doi.org/10.1152/ajpendo.00294.2015. Autophagy.

[8] A. Ali, Y. Zhang, M. Fu, Y. Pei, L. Wu, R. Wang, G. Yang, Cystathionine gamma-lyase/H2S system suppresses hepatic acetyl-CoA accumulation and nonalcoholic fatty liver disease in mice, Life Sci. 252 (2020) 117661, https://doi.org/10.1016/j.lfs.2020.117661.

[9] G. Cirino, C. Szabo, A. Papapetropoulos, Physiological roles of hydrogen sulfide in mammalian cells, tissues, and organs, Physiol. Rev. 103 (2023) 31–276, https://doi.org/10.1152/physrev.00028.2021.

[10] O. Kabil, R. Banerjee, Enzymology of H2S biogenesis, decay and signaling, Antioxidants Redox Signal. 20 (2014) 770–782, https://doi.org/10.1089/ars.2013.5339.

[11] H. Kimura, Production and physiological effects of hydrogen sulfide, Antioxidants Redox Signal. 20 (2014) 783–793, https://doi.org/10.1089/ars.2013.5309.

[12] W. Xu, C. Cui, C. Cui, Z. Chen, H. Zhang, Q. Cui, G. Xu, J. Fan, Y. Han, L. Tang, G. Targher, C.D. Byrne, M.H. Zheng, L. Yang, J. Cai, B. Geng, Hepatocellular cystathionine γ lyase/hydrogen sulfide attenuates nonalcoholic fatty liver disease by activating farnesoid X receptor, Hepatology 76 (2022) 1794–1810, https://doi.org/10.1002/hep.32577.

[13] S. Mani, H. Li, G. Yang, L. Wu, R. Wang, Deficiency of cystathionine gamma-lyase and hepatic cholesterol accumulation during mouse fatty liver development, Sci Bull (Beijing) 60 (2015) 336–347, https://doi.org/10.1007/s11434-014-0722-7.

[14] A. Katsouda, D. Valakos, V.S. Dionellis, S.I. Bibli, I. Akoumianakis, S. Karaliota, K. Zuhra, I. Fleming, N. Nagahara, S. Havaki, V.G. Gorgoulis, D. Thanos, C. Antoniades, C. Szabo, A. Papapetropoulos, MPST sulfurtransferase maintains mitochondrial protein import and cellular bioenergetics to attenuate obesity, J. Exp. Med. 219 (2022) e20211894, https://doi.org/10.1084/jem.20211894.

[15] A. Katsouda, M. Markou, P. Zampas, A. Varela, C.H. Davos, V. Vellecco, G. Cirino, M. Bucci, A. Papapetropoulos, CTH/MPST double ablation results in enhanced vasorelaxation and reduced blood pressure via upregulation of the eNOS/sGC pathway, Front. Pharmacol. 14 (2023) 1090654, https://doi.org/10.3389/fphar.2023.1090654.

[16] C. Hine, J. Mitchell, Endpoint or kinetic measurement of hydrogen sulfide production capacity in tissue extracts, Bio Protoc 7 (2017) e2382, https://doi.org/10.21769/bioprotoc.2382.

[17] C. Hine, E. Harputlugil, Y. Zhang, C. Ruckenstuhl, B.C. Lee, L. Brace, A. Longchamp, J.H. Treviño-Villarreal, P. Mejia, C.K. Ozaki, R. Wang, V. N. Gladyshev, F. Madeo, W.B. Mair, J.R. Mitchell, Endogenous hydrogen sulfide

production is essential for dietary restriction benefits, Cell 160 (2015) 132–144, https://doi.org/10.1016/j.cell.2014.11.048.
[18] J.D. Horton, J.L. Goldstein, M.S. Brown, SREBPs: activators of the complete program of cholesterol and fatty acid synthesis in the liver, J. Clin. Investig. 109 (2002) 1125–1131, https://doi.org/10.1172/jci200215593.
[19] B. Li, S.Y. Cai, J.L. Boyer, The role of the retinoid receptor, RAR/RXR heterodimer, in liver physiology, Biochim. Biophys. Acta, Mol. Basis Dis. 1867 (2021) 166085, https://doi.org/10.1016/j.bbadis.2021.166085.
[20] Y. Duan, K. Gong, S. Xu, F. Zhang, X. Meng, J. Han, Regulation of cholesterol homeostasis in health and diseases: from mechanisms to targeted therapeutics, Signal Transduct Target Ther 7 (2022) 265, https://doi.org/10.1038/s41392-022-01125-5.
[21] A. Montagner, A. Polizzi, E. Fouché, S. Ducheix, Y. Lippi, F. Lasserre, V. Barquissau, M. Régnier, C. Lukowicz, F. Benhamed, A. Iroz, J. Bertrand-Michel, T. Al Saati, P. Cano, L. Mselli-Lakhal, G. Mithieux, F. Rajas, S. Lagarrigue, T. Pineau, N. Loiseau, C. Postic, D. Langin, W. Wahli, H. Guillou, Liver PPARα is crucial for whole-body fatty acid homeostasis and is protective against NAFLD, Gut 65 (2016) 1202–1214, https://doi.org/10.1136/gutjnl-2015-310798.
[22] X. Xu, K.L. Poulsen, L. Wu, S. Liu, T. Miyata, Q. Song, Q. Wei, C. Zhao, C. Lin, J. Yang, Targeted therapeutics and novel signaling pathways in non-alcohol-associated fatty liver/steatohepatitis (NAFL/NASH), Signal Transduct Target Ther 7 (2022) 287, https://doi.org/10.1038/s41392-022-01119-3.
[23] F.N. Cassim Bawa, Y. Zhang, Retinoic acid signaling in fatty liver disease, Liver Res 7 (2023) 189–195, https://doi.org/10.1016/j.livres.2023.07.002.
[24] M. Pawlak, P. Lefebvre, B. Staels, Molecular mechanism of PPARα action and its impact on lipid metabolism, inflammation and fibrosis in non-alcoholic fatty liver disease, J. Hepatol. 62 (2015) 720–733, https://doi.org/10.1016/j.jhep.2014.10.039.
[25] Z.M. Younossi, A.B. Koenig, D. Abdelatif, Y. Fazel, L. Henry, M. Wymer, Global epidemiology of nonalcoholic fatty liver disease-meta-analytic assessment of prevalence, Incidence, and Outcomes 64 (2015) 73–87, https://doi.org/10.1002/hep.28431/suppinfo.
[26] N. Nagahara, M. Nagano, T. Ito, K. Shimamura, T. Akimoto, H. Suzuki, Antioxidant enzyme, 3-mercaptopyruvate sulfurtransferase-knockout mice exhibit increased anxiety-like behaviors: a model for human mercaptolactate- cysteine disulfiduria, Sci. Rep. 3 (2013) 1986, https://doi.org/10.1038/srep01986.
[27] W. Guo, D. Li, V. You, W. Li, B. Hu, S. Zhang, L. Miao, M. Xian, Y. Zhu, X. Shen, Cystathionine γ-lyase deficiency aggravates obesity-related insulin resistance via FoxO1-dependent hepatic gluconeogenesis, FASEB (Fed. Am. Soc. Exp. Biol.) J. 33 (2019) 4212–4224, https://doi.org/10.1096/fj.201801894R.
[28] J.D. Horton, I. Shimomura, M.S. Brown, R.E. Hammer, J.L. Goldstein, H. Shimano, Activation of cholesterol synthesis in preference to fatty acid synthesis in liver and adipose tissue of transgenic mice overproducing sterol regulatory element-binding protein-2, J. Clin. Investig. 101 (1998) 2331–2339, https://doi.org/10.1172/JCI2961.
[29] H. Shimano, J.D. Horton, R.E. Hammer, I. Shimomura, M.S. Brown, J.L. Goldstein, Overproduction of cholesterol and fatty acids causes massive liver enlargement in transgenic mice expressing truncated SREBP-1a, J. Clin. Investig. 98 (1996) 1575–1584, https://doi.org/10.1172/jci118951.
[30] H. Shimano, J.D. Horton, I. Shimomura, R.E. Hammer, M.S. Brown, J.L. Goldstein, Isoform 1c of sterol regulatory element binding protein is less active than isoform 1a in livers of transgenic mice and in cultured cells, J. Clin. Investig. 99 (1997) 846–854, https://doi.org/10.1172/jci119248.
[31] H.K. Min, A. Kapoor, M. Fuchs, F. Mirshahi, H. Zhou, J. Maher, J. Kellum, R. Warnick, M.J. Contos, A.J. Sanyal, Increased hepatic synthesis and dysregulation of cholesterol metabolism is associated with the severity of nonalcoholic fatty liver disease, Cell Metab. 15 (2012) 665–674, https://doi.org/10.1016/j.cmet.2012.04.004.
[32] J.J. Repa, G. Liang, J. Ou, Y. Bashmakov, J.M. Lobaccaro, I. Shimomura, B. Shan, M.S. Brown, J.L. Goldstein, D.J. Mangelsdorf, Regulation of mouse sterol regulatory element-binding protein-1c gene (SREBP-1c) by oxysterol receptors, LXRalpha and LXRbeta, Genes Dev. 14 (2000) 2819–2830, https://doi.org/10.1101/gad.844900.
[33] S.S. Chambel, A. Santos-Gonçalves, T.L. Duarte, The dual role of Nrf2 in nonalcoholic fatty liver disease: regulation of antioxidant defenses and hepatic lipid metabolism, BioMed Res. Int. 18 (2015) 597134, https://doi.org/10.1155/2015/597134, 2015.
[34] J.K.C. Lau, X. Zhang, J. Yu, Animal models of non-alcoholic fatty liver disease: current perspectives and recent advances, J. Pathol. 241 (2017) 36–44, https://doi.org/10.1002/path.4829.
[35] S. Gallage, J.E.B. Avila, P. Ramadori, E. Focaccia, M. Rahbari, A. Ali, N.P. Malek, Q.M. Anstee, M. Heikenwalder, A researcher's guide to preclinical mouse NASH models, Nat. Metab. 4 (2022) 1632–1649, https://doi.org/10.1038/s42255-022-00700-y.
[36] M. Vacca, I. Kamzolas, L.M. Harder, F. Oakley, C. Trautwein, M. Hatting, T. Ross, B. Bernardo, A. Oldenburger, S.T. Hjuler, I. Ksiazek, D. Lindén, D. Schuppan, S. Rodriguez-Cuenca, M.M. Tonini, T.R. Castañeda, A. Kannt, C.M.P. Rodrigues, S. Cockell, O. Govaere, A.K. Daly, M. Allison, K. Honnens de Lichtenberg, Y.O. Kim, A. Lindblom, S. Oldham, A.C. Andréasson, F. Schlerman, J. Marioneaux, A. Sanyal, M.B. Afonso, R. Younes, Y. Amano, S.L. Friedman, S. Wang, D. Bhattacharya, E. Simon, V. Paradis, A. Burt, I.M. Grypari, S. Davies, A. Driessen, H. Yashiro, S. Pors, M. Worm Andersen, M. Feigh, C. Yunis, P. Bedossa, M. Stewart, H.L. Cater, S. Wells, J.M. Schattenberg, Q.M. Anstee, D. Tiniakos, J.W. Perfield, E. Petsalaki, P. Davidsen, A. Vidal-Puig, Q.M. Anstee, A.K. Daly, S. Cockell, D. Tiniakos, P. Bedossa, A. Burt, F. Oakley, H.J. Cordell, C.P. Day, K. Wonders, P. Missier, M. McTeer, L. Vale, Y. Oluboyede, M. Breckons, J. Boyle, P.M. Bossuyt, H. Zafarmand, Y. Vali, J. Lee, M. Nieuwdorp, A.G. Holleboom, A. Angelakis, J. Verheij, V. Ratziu, K. Clément, R. Patino-Navarrete, R. Pais, V. Paradis, D. Schuppan, J.M. Schattenberg, R. Surabattula, S. Myneni, Y.O. Kim, B.K. Straub, A. Vidal-Puig, M. Vacca, S. Rodrigues-Cuenca, M. Allison, I. Kamzolas, E. Petsalaki, M. Campbell, C.J. Lelliott, S. Davies, M. Orešič, T. Hyötyläinen, A. McGlinchey, J. M. Mato, Ó. Millet, J.F. Dufour, A. Berzigotti, M. Masoodi, N.F. Lange, M. Pavlides, S. Harrison, S. Neubauer, J. Cobbold, F. Mozes, S. Akhtar, S. Olodo-Atitebi, R. Banerjee, E. Shumbayawonda, A. Dennis, A. Andersson, I. Wigley, M. Romero-Gómez, E. Gómez-González, J. Ampuero, J. Castell, R. Gallego-Durán, I. Fernández-Lizaranzu, R. Montero-Vallejo, M. Karsdal, D.G.K. Rasmussen, D.J. Leeming, A. Sinisi, K. Musa, E. Sandt, M.M. Tonini, E. Bugianesi, C. Rosso, A. Armandi, F. Marra, A. Gastaldelli, G. Svegliati, J. Boursier, S. Francque, L. Vonghia, A. Verrijken, E. Dirinck, A. Driessen, M. Ekstedt, S. Kechagias, H. Yki-Järvinen, K. Porthan, J. Arola, S. van Mil, G. Papatheodoridis, H. Cortez-Pinto, A.P. Silva, C. M.P. Rodrigues, L. Valenti, S. Pelusi, S. Petta, G. Pennisi, L. Miele, A. Liguori, A. Geier, M. Rau, C. Trautwein, J. Reißing, G.P. Aithal, S. Francis, N. Palaniyappan, C. Bradley, P. Hockings, M. Schneider, P.N. Newsome, S. Hübscher, D. Wenn, J. Magnanensi, A. Trylesinski, R. Mayo, C. Alonso, K. Duffin, J.W. Perfield, Y. Chen, M.L. Hartman, C. Yunis, M. Miller, Y. Chen, E.J. McLeod, T. Ross, B. Bernardo, C. Schölch, J. Ertle, R. Younes, H. Coxson, E. Simon, J. Gogain, R. Ostroff, L. Alexander, H. Biegel, M.S. Kjær, L.M. Harder, N. Al-Sari, S.S. Veidal, A. Oldenburger, J. Ellegaard, M.M. Balp, L. Jennings, M. Martic, J. Löffler, D. Applegate, R. Torstenson, D. Lindén, C. Fournier-Poizat, A. Llorca, M. Kalutkiewicz, K. Pepin, R. Ehman, G. Horan, G. Ho, D. Tai, E. Chng, T. Xiao, S. D. Patterson, A. Billin, L. Doward, J. Twiss, P. Thakker, Z. Derdak, H. Yashiro, H. Landgren, C. Lackner, A. Gouw, P. Hytiroglou, O. Govaere, C. Brass, An unbiased ranking of murine dietary models based on their proximity to human metabolic dysfunction-associated steatotic liver disease (MASLD), Nat. Metab. 6 (2024) 1178–1196, https://doi.org/10.1038/s42255-024-01043-6.
[37] P.K. Santhekadur, D.P. Kumar, A.J. Sanyal, Preclinical models of non-alcoholic fatty liver disease, J. Hepatol. 68 (2018) 230–237, https://doi.org/10.1016/j.jhep.2017.10.031.
[38] E. Smagris, S. Basuray, J. Li, Y. Huang, K.-M.V. Lai, J. Gromada, J.C. Cohen, H. H. Hobbs, Pnpla3I148M Knockin Mice Accumulate PNPLA3 on Lipid Droplets and Develop Hepatic Steatosis, vol. 61, 2014, pp. 108–118, https://doi.org/10.1002/hep.27242/suppinfo.
[39] A. Cast, M. Kumbaji, A.D. Souza, K. Rodriguez, A. Gupta, R. Karns, L. Timchenko, N. Timchenko, Liver proliferation is an essential driver of fibrosis in mouse models of nonalcoholic fatty liver disease, Hepatol Commun 3 (2019) 1036–1049, https://doi.org/10.1002/hep4.1381/suppinfo.